


 Cite this: *RSC Adv.*, 2025, 15, 44102

# Highly emissive dinuclear europium(III) complex with heteroaryl $\beta$ -diketone and fluxidentate pyrazine: dual role as UV converters and semiconductors

 Vandana Aggarwal,<sup>a</sup> Devender Singh,<sup>b</sup> \*<sup>ab</sup> Sofia Malik,<sup>a</sup> Shri Bhagwan,<sup>a</sup> Sumit Kumar,<sup>c</sup> Rajender Singh Malik,<sup>c</sup> Parvin Kumar<sup>d</sup> and Jayant Sindhu<sup>e</sup>

Single component red light emissive complexes with single emissive centers are emerging as promising color converters for light emitting diodes (LEDs). In this work, a thiophene-based  $\beta$ -diketone ligand, 4,4,4-trifluoro-1-(2-thienyl)-1,3-butanedione (TTBD), featuring a trifluorobutane group at the opposite position, was used to develop a dinuclear Eu(III) complex,  $\text{Eu}_2(\text{TTBD})_6\text{pyz}$  (EuD), where pyz refers to pyrazine. Additionally, its mononuclear counterpart (EuM) and a binary analogue (EuA) were also prepared for comparative studies. The complexes were thoroughly characterized using IR, NMR, UV-vis, photoluminescence (PL) spectroscopy and thermogravimetric analysis (TGA). Experimental results demonstrated that a dinuclear Eu(III) complex displays excellent thermal stability and broad, strong excitation bands spanning 200–350 nm, monitored at the characteristic 612 nm emission. Under near-UV light excitation, the complex shows intense red luminescence, attributed to f–f transitions of the central Eu(III) ions. Importantly, red emission intensity of the dinuclear complex is significantly higher than its mononuclear analogues, indicating a synergistic effect between the two Eu(III) centers. The lack of ligand based emission in all complexes suggests efficient energy transfer from the attached sensitizer to the Eu(III) ion. Based on the emission spectrum, the CIE chromaticity coordinates ( $x = 0.63$ ,  $y = 0.34$ ) confirm the suitability of the complex as an effective red phosphor for white LED applications. The fluorescence lifetime measurements, along with estimation of triplet energy ( $T_1$ ) level of TTBD (20 600  $\text{cm}^{-1}$ ), which is higher than the  $^5\text{D}_0$  excitation level of Eu(III), support a ligand sensitized luminescence mechanism *i.e.* antenna effect. This conclusion is further supported by theoretical (JOES) and computational (DFT) studies, which also provided insights into the electronic density distribution. Altogether, these findings validate the potential of the synthesized complexes, particularly the dinuclear system, as efficient red components for integration in near-UV pumped white LEDs.

 Received 15th September 2025  
 Accepted 6th November 2025

DOI: 10.1039/d5ra06968h

[rsc.li/rsc-advances](http://rsc.li/rsc-advances)

## 1. Introduction

Lanthanide complexes have gained considerable attention in recent years due to their exceptional prospects across a wide range of technological arenas. Lanthanide ions such as Eu(III), Tb(III), Gd(III), Dy(III) and Sm(III) possess unique electronic configurations arising from their f-orbitals, which enable them

to exhibit distinctive electronic and luminescent behaviors. When coordinated with suitable organic ligands, these ions form stable complexes capable of multicolor emission, making them highly attractive for uses in optoelectronics,<sup>1</sup> biomedical imaging,<sup>2</sup> materials science<sup>3</sup> and device engineering.<sup>4</sup> Despite their intrinsically low oscillator strengths resulting from Laporte forbidden transitions, lanthanide excited states can be efficiently populated *via* energy transfer from organic chromophores.<sup>5</sup> The unable nature of their electronic properties, through the selection of specific metal ions and ligand systems, opens the door to the development of advanced functional materials. Tailoring ligands with various donor atoms and distinct electron distributions enables precise control of energy transfer mechanisms and luminescent behavior. This versatility positions lanthanide complexes as valuable components in molecular electronics, sensors, catalysts and magnetic materials.

<sup>a</sup>Department of Chemistry, Maharshi Dayanand University, Rohtak-124001, Haryana, India. E-mail: devjakhar@gmail.com

<sup>b</sup>Department of Chemistry, Lovely Professional University, Phagwara, Jalandhar, 14441, Punjab, India

<sup>c</sup>Department of Chemistry, DCR University of Science & Technology, Murthal-131039, Haryana, India

<sup>d</sup>Department of Chemistry, Kurukshetra University, Kurukshetra-136119, Haryana, India

<sup>e</sup>Department of Chemistry, COBS&H, CCS Haryana Agricultural University, Hisar-125004, Haryana, India


Within this domain, homodinuclear lanthanide complexes have emerged as especially promising due to their enhanced properties compared to mononuclear analogues. Metal–metal interactions in dinuclear systems can boost luminescence, offering improved performance in light emitting applications. The present study investigates a dinuclear europium complex synthesized alongside monometallic and binary variants to evaluate its enhanced luminescent properties and efficiency. Designing highly emissive lanthanide complexes requires a detailed understanding of the energy transfer processes, particularly from the singlet ( $^1\pi\pi^*$ ) and triplet ( $^3\pi\pi^*$ ) states of the ligands to the  $^5D_0$  level of Eu(III) ion, where characteristic emission occurs.<sup>6</sup> Fluorinated ligands can lower the triplet energy level, facilitating efficient energy transfer *via*  $T_1$  state of ligand, a process that may include reverse intersystem crossing. Research into lanthanide coordination complexes, especially those involving  $\beta$ -diketones and polyazine-based ligands, has expanded significantly. Polyazine ligands are especially effective as bridging units that link lanthanide centers, enhancing stability and functionality of the resulting complexes.<sup>7</sup>

This study presents the first structural characterization of a homodinuclear europium complex bridged by pyrazine (pyz), a polyazine ligand. The complex,  $[\text{Eu}(\text{TTBD})_3]_2\text{pyz}$ , incorporates 4,4,4-trifluoro-1-(2-thienyl)-1,3-butanedione (TTBD) as terminal ligand, known for its excellent light harvesting capabilities. Thermal stability and luminescent properties of this bridged complex have been analyzed and compared with its monometallic and binary counterparts. Three europium complexes were synthesized and studied: two eight coordinated species,  $[\text{Eu}(\text{TTBD})_3(\text{H}_2\text{O})_2]$  (EuA) and  $[\text{Eu}(\text{TTBD})_3(\text{pyz})_2]$  (EuM), where water and pyz act as monodentate co-ligands, and one seven coordinated homodinuclear complex,  $[\text{Eu}_2(\text{TTBD})_6(\text{pyz})]$  (EuD), in which pyz serves as a bridging ligand/spacer. These are summarized in Table 1.

## 2. Materials

Pyrazine, TTBD and  $\text{EuCl}_3 \cdot 6\text{H}_2\text{O}$  (99.99%) were obtained from Sigma (SA) and used without further purification. All solvents employed, including 25% aqueous ammonia solution, ethanol and hexane, were used as received without additional distillation.

## 3. Techniques

Elemental analysis was made using PerkinElmer 2400 CHN analyzer. Infrared profiles were noted on PerkinElmer 5700 FTIR spectrophotometer in mid IR region ( $4000\text{--}400\text{ cm}^{-1}$ ), using anhydrous potassium bromide pellets as reference. <sup>1</sup>H

NMR spectra were obtained using an Bruker Avance FT NMR spectrometer, with tetramethylsilane (TMS) as the internal reference and deuterated chloroform ( $\text{CDCl}_3$ ) as the solvent. UV visible absorption spectra (200–600 nm) were recorded in dichloromethane (DCM) using a Shimadzu UV-2450 spectrophotometer. Optical bandgap energies were estimated using Tauc plots derived from the absorption data. Photoluminescence (PL) measurements were performed on a Horiba Jobin Yvon Fluorolog FL-3-11 spectrofluorometer. Luminescence decay profiles were recorded on Hitachi F-7000 FL spectrophotometer equipped with a Xe lamp. Chromaticity coordinates were calculated from the PL emission data using a standard color calculator. Thermal stability was analyzed using a Hitachi STA-7300 thermal analyzer under  $\text{N}_2$  atmosphere, at a heating rate of  $10\text{ }^\circ\text{C min}^{-1}$ . These analyses were made at room temperature unless stated otherwise.

## 4. Synthesis

Europium complexes with the general formula  $[\text{Eu}(\text{TTBD})_3(\text{L})_2]$ , where  $\text{L} = \text{H}_2\text{O}$  or pyz and  $[\text{Eu}_2(\text{TTBD})_6(\text{L})]$  were synthesized following the procedures illustrated in Fig. S1–S3 (in SI) for EuA,<sup>8,9</sup> EuM<sup>10,11</sup> and EuD,<sup>12,13</sup> respectively.

## 5. Results and discussions

### 5.1 Elemental study

The physical appearance, elemental analysis data and molecular formulas of the synthesized complexes are summarized in Table 1. All complexes display good solubility in common organic solvents such as dichloromethane (DCM), chloroform and dimethyl sulfoxide (DMSO).<sup>14</sup> The experimental elemental analysis results (exp.) are in close agreement with the theoretically calculated values (theo.), confirming both the purity and the successful synthesis of the complexes. Furthermore, the data support the formation of the complexes in the expected stoichiometric ratios.

### 5.2 IR study

Infrared profiles of prepared europium complexes were taken to detect the coordination between ligands and the metal ion. A notable shift in the carbonyl ( $\nu_{\text{C=O}}$ ) stretching vibration from  $\sim 1655\text{ cm}^{-1}$  in uncoordinated TTBD ligand<sup>15</sup> to  $1605\text{ cm}^{-1}$  in  $\text{Eu}(\text{TTBD})_3 \cdot 2\text{H}_2\text{O}$  complex indicates coordination of ligand to Eu(III) ion *via* carbonyl oxygen. In synthesized complexes, this  $\nu_{\text{C=O}}$  band undergoes further shifts to  $1601\text{ cm}^{-1}$  in EuM and  $1603\text{ cm}^{-1}$  in EuD, providing clear evidence that coordination persists in these systems. These shifts suggest that the  $\beta$ -

Table 1 % CHN content in EuA–EuD

Complex	Color	$C_{\text{exp.}}$ (theo.)	$H_{\text{exp.}}$ (theo.)	$N_{\text{exp.}}$ (theo.)	Formula
EuA	White	33.93 (33.85)	1.76 (1.89)	— (—)	$\text{C}_{24}\text{H}_{16}\text{EuF}_9\text{O}_8\text{S}_3$
EuM	White	39.46 (39.39)	2.14 (2.07)	5.76 (5.74)	$\text{C}_{32}\text{H}_{20}\text{EuF}_9\text{N}_4\text{O}_6\text{S}_3$
EuD	White	35.99 (36.50)	1.49 (1.65)	1.68 (1.64)	$\text{C}_{52}\text{H}_{28}\text{Eu}_2\text{F}_{18}\text{N}_2\text{O}_{12}\text{S}_6$



Table 2 IR stretch of EuA–EuD (in  $\text{cm}^{-1}$ )

Complex	TTBD	pyz	EuA	EuM	EuD
$\nu_{(\text{Eu}-\text{O})}$	—	—	459	455	458
$\nu_{(\text{Eu}-\text{N})}$	—	—	—	583	581
$\nu_{(\text{C}-\text{F})}$	—	—	1141, 1192	1139, 1191	1140, 1191
$\nu_{(\text{C}-\text{N})}$	—	—	—	1358	1360
$\nu_{(\text{C}=\text{C})}$	—	1457	1447, 1458	1412, 1458	1437, 1458
$\nu_{(\text{C}=\text{N})}$	—	—	—	1541	1538
$\nu_{(\text{C}=\text{O})}$	1655	—	1605	1601	1603
$\nu_{(=\text{CH})}$	—	—	3123	3124	3127

diketonate ligand remains coordinated to Eu(III) center and that pyz interacts to form a new coordination environment, where the C=N bond is involved in coordination, likely resulting in a C=N–Eu–O type coordination motif. Additional confirmation comes from shifts observed in the C=N stretching vibrations of pyrazine, which are displaced to  $1541\text{ cm}^{-1}$  in EuM and  $1538\text{ cm}^{-1}$  in EuD, further supporting coordination of the nitrogen atom in pyz to the europium center. These changes, along with modifications observed in other ligand related vibrational bands (summarized in Table 2), emphasize the formation of the desired complexes. Importantly, the broad O–H stretching band typically observed around  $3500\text{ cm}^{-1}$  present in EuA due to coordinated water molecules is absent in the spectra of both EuM and EuD.<sup>16</sup> This confirms the replacement of water by pyz ligand and indicates that EuM and EuD are anhydrous. A distinct band near  $460\text{ cm}^{-1}$  in prepared complexes is assigned to Eu–O stretch, confirming coordination of TTBD ligand to Eu(III).<sup>17</sup> Additionally, a shoulder  $\sim 580\text{ cm}^{-1}$ , attributed to Eu–N stretching, provides confirmation for bonding of pyz to Eu(III) ion.<sup>17</sup> A further band near  $560\text{ cm}^{-1}$  occurs due to out-of-plane ring bending vibrations of the TTBD. In the IR spectrum (in  $\text{cm}^{-1}$ ) of free pyz, characteristic bands are observed at 3155 and 3059 (aromatic C–H stretching), 1709 and 1522 (C=C and C=N vibrations), 1408 (ring vibrations), 1149, 1130 and 1062 (C–H bending), 1020–1005 (ring vibrations) and a strong band at 787 (out-of-plane C–H bending).<sup>18</sup> Upon coordination with Eu(TTBD)<sub>3</sub>, many of these bands diminish or disappear in the complex spectra, particularly in EuM, where only a prominent band at  $1401\text{ cm}^{-1}$  remains. This suggests selective coordination of one nitrogen atom in pyrazine, altering its symmetry and vibrational profile. Specifically, a band appearing between  $940\text{--}1010\text{ cm}^{-1}$  is indicative of reduced molecular symmetry in coordinated pyrazine. EuM displays a band at  $944\text{ cm}^{-1}$ , which is different from that of EuD, supporting the coordination of pyrazine *via* single N-atom in EuM.<sup>19</sup> This observation is consistent with the formation of a mono coordinated pyz complex in EuM, while a different coordination pattern is likely present in EuD.

### 5.3 <sup>1</sup>H NMR study

Proton magnetic resonance (PMR) spectroscopy is utilized to verify the successful formation of the expected mono and dinuclear complexes (EuA, EuM and EuD). The results aligned with the structural expectations of single and dual metal centers

Table 3 PMR peaks (in ppm) of EuA–EuD

Complex	Peaks (TTBD)	Peaks (pyz)
Free	14.9 (1H), 7.84 (1H), 7.60 (1H), 7.20 (1H), 6.45 (1H)	8.50 (4H)
EuA	3.01 (s), 6.24–7.49 (m)	—
EuM	2.92 (s), 6.19–7.41 (m)	6.77 (s), 10.63 (s)
EuD	2.53 (s), 6.17–6.78 (m)	9.54 (s)

in EuA/EuM and EuD, individually (Table 3). Different spectral characteristics were observed: uncoordinated pyz produced a sharp singlet around 8.50 ppm,<sup>20</sup> whereas TTBD showed peaks at 14.9, 7.84, 7.60, 7.20 and 6.45 ppm, due to the O–H proton, 3 aromatic protons of the thienyl ring and the methine proton, individually.<sup>21</sup> In the case of EuM, two symmetrical peaks of equal intensity were detected for the pyz at 6.77 and 10.63 ppm. These shifts suggest that protons closer to the Eu(III) ion experienced higher  $\delta$  values, while those further away shifted to lower values. Presence of two equally intense pyrazine peaks supports coordination through a single nitrogen atom. The stoichiometry, coordination of two pyrazine ligands and three TTBD ligands to Eu(III), was corroborated by the proton signal intensity ratio between TTBD and pyrazine, indicating an eight coordinate metal center. Significant chemical shift changes were observed: methine protons in EuM shifted downfield compared to free TTBD and pyrazine protons experienced opposite direction shifts in  $\delta$  values. This contrast highlights the dipolar nature of paramagnetic shifts, as explained by eqn (1):<sup>22</sup>

$$A_p = D_1 \left( \frac{3 \cos^2 \theta - 1}{r^3} \right) \quad (1)$$

Here, all variables possess their conventional meanings. The extent of paramagnetic shift is inversely related to distance between the paramagnetic metal ion and the proton, resulting in greater shifts for protons closer to the Eu(III) center. For EuD, PMR spectra exhibited three distinct peaks, approving the bridging mode of one pyz molecule to two [Ln(TTBD)<sub>3</sub>] units, thereby resulting a seven coordinate Ln(III) system. In this complex also, methine and phenyl protons from TTBD shifted in opposite directions, further supporting the dipolar character of the paramagnetic shift. EuA displayed three main PMR signals: a sharp singlet for three methine protons of TTBD, a multiplet ranging 6.24–7.49 ppm for the nine aryl protons and an additional signal attributed to coordinated water molecules. Based on the combined outcomes of CHN, IR and NMR analysis, the proposed structures of EuA–EuD are displayed in Fig. 1.

### 5.4 UV-vis study

Electronic absorption spectra of TTBD and its europium complexes are depicted in Fig. 2.  $\beta$ -Diketonate unit within the complexes exhibits a singlet–singlet  $n\text{--}\pi^*$  enolic transition, which is primarily responsible for the antenna effect that facilitates the photoluminescent behavior of the europium complexes.<sup>23</sup> In contrast, the contribution of  $\pi\text{--}\pi^*$  transitions



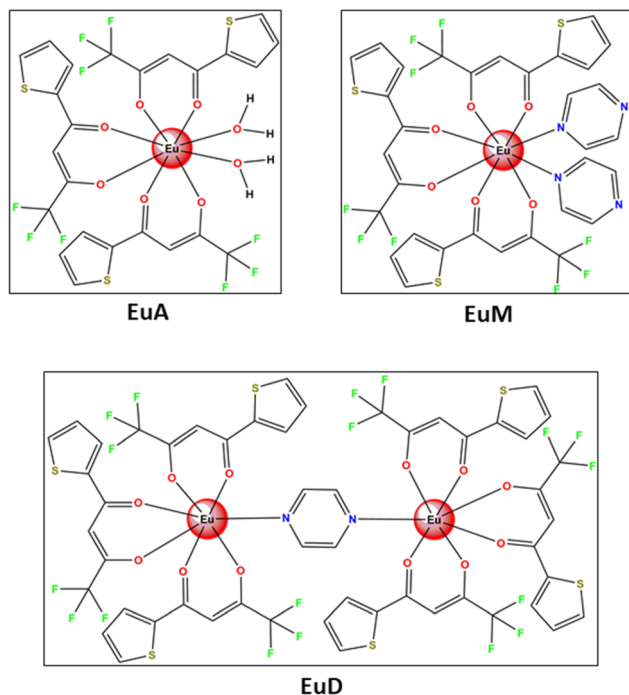


Fig. 1 Structure of EuA–EuD.

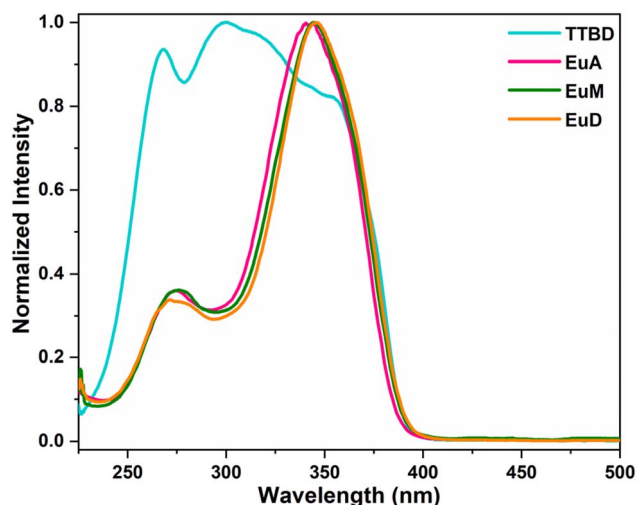


Fig. 2 Normalized electronic absorption spectral profiles of TTBD and EuA–EuD.

from the pyrazine ligand is minimal due to the electronic configuration of Eu(III), which is  $[\text{Xe}]4f^6$ , containing six unpaired electrons. The electronic states of free Eu(III) ion are represented

by the  ${}^7F_J$  term symbols ( $J = 4, 3, 2, 1, 0$ ) and emissions from the excited  ${}^5D_0$  state to these  ${}^7F_J$  levels occur in the visible spectrum. All the Eu(III) complexes display absorption features closely resembling those of TTBD, though the absorption edge in the complexes shifts slightly toward the near-UV region, extending into the 350–400 nm range. This strong absorption is primarily ascribed to  $\pi$ – $\pi^*$  transitions within aromatic chromophores and the ligand frameworks of the complexes. EuA complex shows a maximum absorption band at 342 nm, while EuM and EuD exhibit a similar band around 344 nm, indicating that changes in nuclearity do not significantly impact the absorption characteristics. This consistency likely arises from the use of the same ligands (pyrazine and TTBD) across all complexes. The lack of significant shifts in absorption peaks or changes in band shape suggests that these ligands are the main absorbers of UV light and that the Eu(III) ion itself does not significantly absorb in this region. Furthermore, no intraconfigurational f–f transitions are observed in the absorption profiles within this spectral range. The coordination of the spacer in the EuD complex not only increases absorption intensity but also contributes to achieving a higher coordination number for the central Eu(III) ion. This leads to greater coordination saturation, thereby enhancing the thermal stability of the dinuclear europium complexes.<sup>24</sup> The calculated absorption maxima for these complexes are listed in Table 4. The optical band gaps  $E_g$  were determined by transforming the UV-vis absorption data (Fig. 2) using Tauc method.<sup>25</sup> The Tauc relation is expressed as (eqn 2):<sup>26</sup>

$$\alpha h\nu = A(h\nu - E_g)^n \quad (2)$$

Here,  $\alpha$  is molar absorptivity,  $h\nu$  is photon energy,  $A$  is electronic tailing coefficient and  $n$  is nature of the electronic transition (direct or indirect). For analysis,  $(\alpha h\nu)^2$  is plotted against  $h\nu$  and  $E_g$  is estimated by extrapolating the linear portion of the curve to intersect the energy axis where  $(\alpha h\nu)^2 = 0$ . Resulting values are given in Table 4, with corresponding Tauc plots displayed in Fig. 3.

## 5.5 Photoluminescence spectroscopy

**5.5.1 PL excitation and emission.** Excitation spectra were obtained by monitoring the emission at 612 nm (Fig. 4). These spectra display two weak intraconfigurational f–f transitions, specifically at 464 nm ( $21\,551\text{ cm}^{-1}$ , due to the  ${}^5D_2 \leftarrow {}^7F_0$  transition) and 533 nm ( $18\,761\text{ cm}^{-1}$ ,  ${}^5D_1 \leftarrow {}^7F_1$ ) (Table 5).<sup>27</sup> Additionally, two prominent absorption bands appear at 249, 286 for EuA, 242, 283 for EuM and 249, 285 for EuD, which is attributed to  $S_0 \rightarrow S_1$  transition in the chromophores. The

Table 4 Various photosensitive features of EuA–EuD

Complex	$\lambda_{\text{abs}}$ (nm)	$E_g$ (eV)	$\lambda_{\text{ex}}$ (nm)	$\lambda_{\text{em}}$ (nm)	Lifetime (ms)	Quantum yield (%)
EuA	342	3.283	249, 286	612	0.394	26
EuM	344	3.266	242, 283	612	0.605	47
EuD	345	3.254	249, 285	612	0.647	54



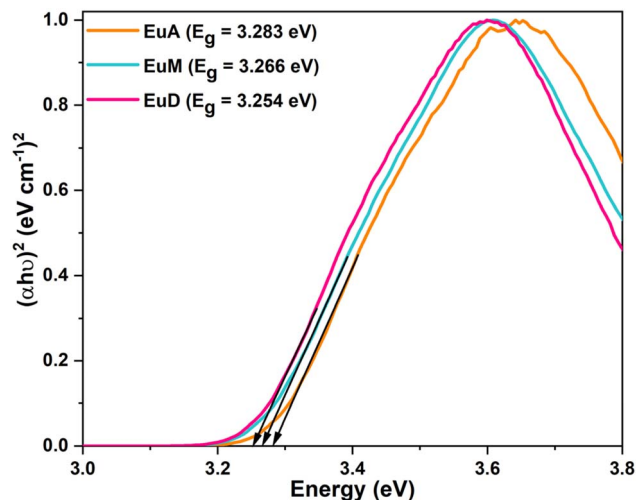


Fig. 3 Tauc's profiles of EuA–EuD.

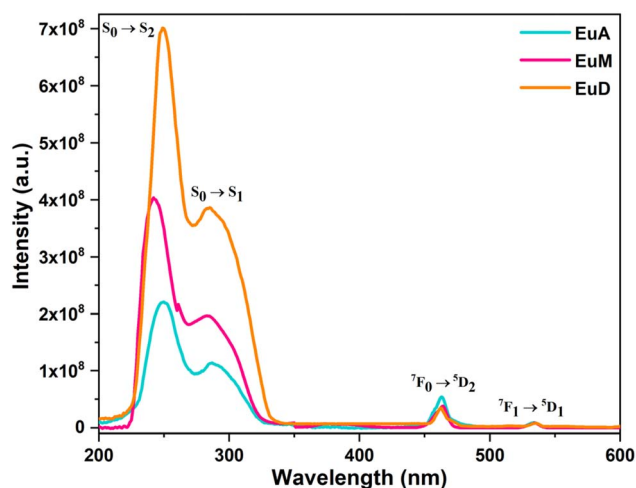


Fig. 4 Excitation graphs of EuA, EuM and EuD in DCM.

Table 5 Metal based excitation peaks in prepared complexes

Transition	Wavelength (nm)
${}^7F_0 \rightarrow {}^5D_2$	464
${}^7F_1 \rightarrow {}^5D_1$	533

presence of a strong ligand centered  $\pi$ - $\pi^*$  excitation band highlights high UV absorption capability of the sensitizing ligands, indicating effective energy transfer potential to emissive state of Eu(III) ion.<sup>28</sup> The excitation spectra of mononuclear and dinuclear complexes exhibit similar overall shapes, regardless of mode of coordination of attached ligand. However, the dinuclear complex (EuD) absorbs significantly more UV radiation and shows greater excitation to higher energy states compared to its mononuclear counterparts. This is likely due to the higher number of absorbing units in EuD

Table 6  $T_1$  energy alongside their gap with emitting level of Eu(III) ion

Moiety	Energy ( $\text{cm}^{-1}$ )
$E_{\text{pyz}}$	26 820
$E_{\text{TTBD}}$	20 600
$E_{\text{Eu(III)}}$	17 241
$\Delta E_{\text{TTBD-Eu(III)}}$	3359
$\Delta E_{\text{pyz-Eu(III)}}$	9579

approximately seven compared to three to five in the mononuclear complexes.

Emission spectra were recorded over the 400–720 nm range under optimized excitation conditions (Fig. 5). The spectra for the synthesized europium complexes exhibit five distinct emission bands, which correspond to transitions from the excited  ${}^5D_0$  state to the  ${}^7F_J$  levels ( $J = 0, 1, 2, 3$  and 4) of the Eu(III) ion, appearing approximately at 578, 593, 612, 653 and 701 nm.<sup>29</sup> The similarity across the spectra indicates that the luminescent centers in all complexes are essentially the same. The most intense emission band is the ED (electric dipole) transition  ${}^5D_0 \rightarrow {}^7F_2$  near 612 nm, which is primarily responsible for the characteristic red emission of these complexes.<sup>30</sup> This strong emission is attributed to the asymmetric and saturated coordination geometry surrounding the Eu(III) ion. While intensity of MD (magnetic dipole)  ${}^5D_0 \rightarrow {}^7F_1$  transition is not significantly influenced by the surrounding chemical environment, its splitting into Stark components provides insights into the symmetry around the Eu(III) ion. However, in solution phase, this Stark splitting is not observed. Furthermore, ratio of the ED to MD peak intensities for EuA, EuM and EuD are 15.28, 18.19 and 3.26, respectively (Table 8), implying that the Eu(III) ions reside in asymmetric environments.<sup>31</sup> The ED transition intensities for these complexes are  $2.09 \times 10^9$ ,  $3.67 \times 10^9$  and  $8.39 \times 10^9$ , respectively. Replacing water molecules in  $[\text{Eu}(\text{TTBD})_3(\text{H}_2\text{O})_2]$  with pyrazine leads to a significant  $\sim 4$  fold increase in luminescence intensity. Moreover, the strong intensity of this transition in the dinuclear complex is due to the ligand field effects and the highly polarizable environment surrounding Eu(III) ion. This enhancement is likely due to the elimination of high frequency O–H vibrations, which typically cause nonradiative energy losses. Notably, dinuclear EuD exhibits stronger emission than EuA and EuM. Shape of the hypersensitive transition bands in this complex (Fig. 5) resembles those of typical seven coordinate Eu(III)  $\beta$ -diketonate complexes in non-coordinating solvents, supporting the idea that EuD retains a seven coordinate structure in solvents.

Moreover, the observation of a single peak of the non-degenerate  ${}^5D_0 \rightarrow {}^7F_0$  transition around 593 nm suggests that only one type of Eu(III) environment is present in the dinuclear complex  $[\text{Eu}(\text{TTBD})_3(\mu\text{-pyz})\text{Eu}(\text{TTBD})_3]$ , indicating a single species in solution.<sup>32</sup> This conclusion is further supported by NMR data, which show a single set of resonances for both the  $\beta$ -diketonate and pyrazine ligands, confirming the equivalency of the Eu(III) sites. It is well known that the energy and intensity of specific Eu(III) emission transitions depend on the nature and configuration of ligands in the first coordination sphere.



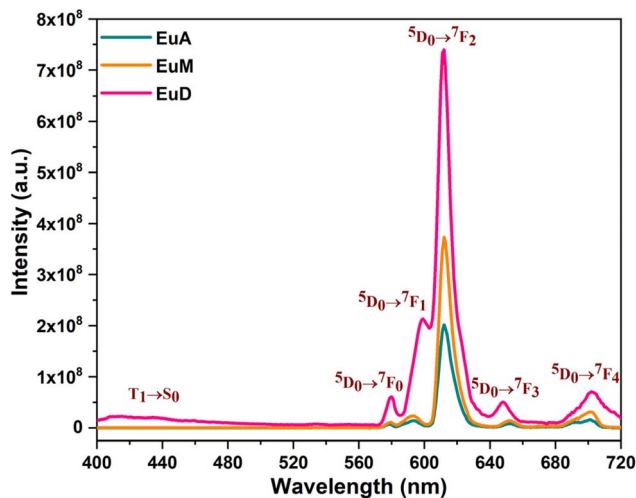


Fig. 5 Emission graphs of EuA–EuD in DCM.

Emission spectra of the prepared complexes with different coordination modes exhibit similar shapes, as evidenced by their overlap; however, the emission intensity for EuA and EuM is noticeably lower than for EuD. This difference likely arises from a lower number of antenna ligands in the former, which reduces energy transfer to the Eu(III) center. Additionally, in EuA, coordinated water molecules act as quenchers due to the high energy O–H vibrations, leading to reduced sensitization. Therefore, the mononuclear complexes exhibit weaker luminescence compared to the dinuclear complex. Furthermore, the phosphorescence spectra of [Gd(TTBD)<sub>3</sub>] and [Gd(py<sub>2</sub>)<sub>3</sub>] complexes at 77 K (Fig. S4 and S5, respectively, in SI) have been noted and color contribution of each peak in emission spectra of prepared complexes is displayed in Fig. S6, in SI.

**5.5.2 Quantum yield.** Photoluminescence quantum yield, the ratio of number of photons emitted to number of photons absorbed, of prepared complexes was noted in DCM.<sup>33</sup> It helped to analyze the effect of coordination environment on the photoluminescence intensity of metal center. It was calculated using eqn (3) against quinine bisulphate as reference in dil. sulphuric acid having quantum yield of 0.546.<sup>34,35</sup>

$$\phi_s = \frac{\phi_r A_r I_r n_s^2}{A_s I_r n_r^2} \quad (3)$$

where, r and s are for reference and unknown sample, respectively.  $I$  is integrated intensity of emission,  $A$  is absorbance at  $\lambda_{\text{ex}}$  and  $n$  is refractive index. Notably high quantum yield value for EuD indicates a significant sensitizing effect of TTBD over pyz for Eu(III) ion in prepared complexes. The obtained data is summarized in Table 4. The relative quantum yields are reported relative to a reference solution with a 20% error margin. The emission quantum yields for the complexes were found to be comparable to those reported previously for similar complexes.<sup>36,37</sup>

In a study performed by Divya and co-workers in 2013, it was reported that the solid state quantum yield of [Eu(pfppd)<sub>3</sub>(tpy)] is found to be the highest so far reported in the literature under

blue light excitation (415 nm) *i.e.* 75%.<sup>38</sup> It is worthy to mention that the quantum yield of EuM and EuD is significantly higher than [Eu(hfaa)<sub>3</sub>(imp)<sub>2</sub>] and [Eu(dbm)<sub>3</sub>(imp)].<sup>39</sup> The higher quantum efficiency indicates that the environment around the Eu(III) in EuM and EuD is favorable for the efficient desired radiative decay. The higher quantum efficiency could be related to the presence of greater C–F bonds and absence of =CH oscillators in TTBD as compared to hfaa and dbm. The emission spectra of EuM do not show any ligand fluorescence whereas it could be seen in the spectrum in the chloroform spectra of [Eu(dbm)<sub>3</sub>(imp)] and [Eu(hfaa)<sub>3</sub>(imp)<sub>2</sub>]. The absence of ligand fluorescence in EuM prompts us to believe efficient energy transfer. The quantum efficiency of present complexes have been found much higher as compared to [Eu(tfaa)<sub>3</sub>(phen)] and [Eu(tfaa)<sub>3</sub>(bpy)].<sup>39</sup> Several studies have explored dinuclear lanthanides and transition metal complexes, there are a few reports on dinuclear Eu(III) complexes with high quantum yields. It is expected, however, that dinuclear Ln(III) complexes would exhibit low symmetry due to the compact structures around the Ln ions, which may result in markedly elevated quantum yields and extended emission lifetimes. These are the fundamental requirements for any luminescent complexes to be used as emissive components in OLEDs and other sensing applications.

**5.5.3 Emission mechanism.** In lanthanide complexes, energy transfer typically proceeds *via* triplet state of ligand.<sup>40</sup> Understanding how this transfer occurs is essential for elucidating the excited state dynamics. Two primary mechanisms govern this transfer: Förster type (dipole–dipole interactions)<sup>41</sup> and Dexter type (electron exchange).<sup>42</sup> Förster mechanism involves long range interactions between the excited donor and acceptor, while Dexter requires orbital overlap and is thus more distance sensitive. For successful Dexter transfer, the donor (ligand) emission must overlap with the acceptor (lanthanide ion) absorption spectrum. In this system, energy transfer likely proceeds from the triplet state of pyz to that of TTBD and then onto the Eu(III) ion, indicating intramolecular energy transfer. Upon light absorption by the organic ligands (*e.g.*, TTBD or pyz), energy is transferred through their triplet states to populate the <sup>5</sup>D<sub>0</sub> emitting level of Eu(III), which then relaxes to the ground state *via* characteristic f–f transitions. The excited state energy levels of Eu(III) <sup>5</sup>D<sub>3</sub> (24 800 cm<sup>-1</sup>), <sup>5</sup>D<sub>2</sub> (21 500 cm<sup>-1</sup>), <sup>5</sup>D<sub>1</sub> (19 100 cm<sup>-1</sup>) and <sup>5</sup>D<sub>0</sub> (17 241 cm<sup>-1</sup>)<sup>43</sup> are populated *via* internal conversion. For efficient sensitization, the ligand triplet energy level must be well aligned with the <sup>5</sup>D<sub>0</sub> level. For instance, TTBD exhibits singlet and triplet levels at 20 600 cm<sup>-1</sup> and 25 164 cm<sup>-1</sup>, respectively, positioning it well for energy transfer to Eu(III) ion.<sup>44</sup> The energy gap ( $\Delta E = E_{T_1} - E_{^5D_0}$ ) for these ligands falls within the ideal 2500–5000 cm<sup>-1</sup> range, as supported by Latva empirical criteria,<sup>45</sup> ensuring high transfer efficiency while minimizing back transfer (Table 6). No significant ligand centered emissions are observed in the 400–520 nm range of the PL spectra (Fig. 5), indicating efficient energy transfer into <sup>5</sup>D<sub>0</sub> level of Eu(III) without emission loss. This also confirms the absence of reverse energy transfer. Additionally, the incorporation of fluorinated ligands is known to reduce vibronic quenching, further improving the overall efficiency of



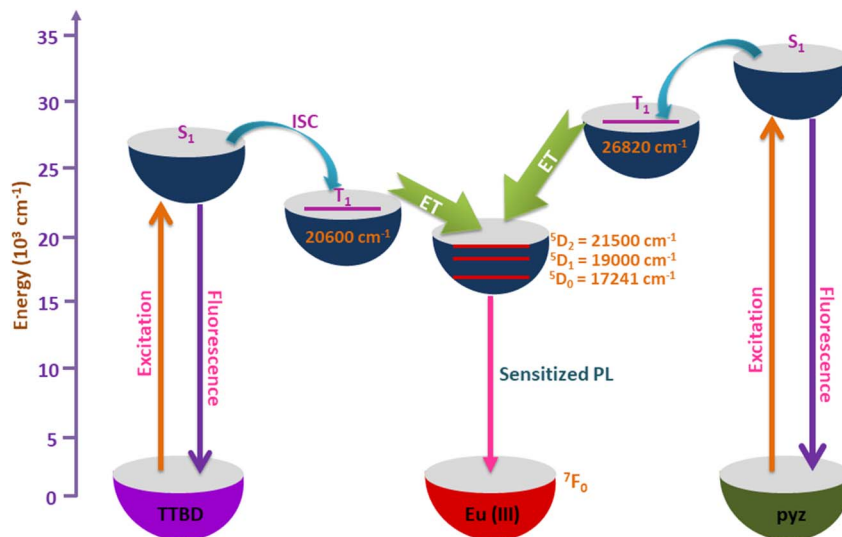


Fig. 6 Probable energy transfer pathway in prepared complexes.

sensitization. Within this system, TTBD singlet and triplet states may serve as bridging states, aiding energy transfer from pyrazine to Eu(III) ion. This relay like mechanism ensures smooth and effective intramolecular energy transfer, resulting in strong red emission *via*  ${}^5D_0 \rightarrow {}^7F_2$  transition. A schematic depiction of this energy transfer pathway is shown in Fig. 6.

**5.5.4 Decay time.** Fluorescence lifetime is a crucial parameter when considering practical applications of luminescent materials, as in FRET systems.<sup>46</sup> PL decay time represents the average duration that a molecule remains in its lowest excited state before emitting a photon *via* radiative relaxation.<sup>47</sup> Emission decay curves of prepared complexes were recorded in the solid state and monitored at their respective excitation and emission wavelengths. As shown in Fig. 7, these curves associated with  ${}^5D_0$  excited state of the Eu(III) ion exhibit mono exponential behavior, indicating a single dominant

luminescent species or multiple Eu(III) ions situated in similar coordination environments. The measured fluorescence lifetimes for EuA, EuM and EuD were found to be 0.394 ms, 0.605 ms and 0.647 ms, respectively. This behavior is mathematically described by eqn (4).<sup>48</sup>

$$T(t) = I_0 + A_1 \exp(-t/\tau) \quad (4)$$

Here,  $A_1$  is pre-exponential factor obtained from the curve fitting,  $I_0$  is initial intensity at  $t = 0$  ms and  $\tau$  is fluorescence lifetime derived from mono exponential decay model. These values indicate that emitting Eu(III) ions reside in a uniform chemical environment. A summary of the absorption and PL data is provided in Table 4. The lifetime of present complexes is shorter than the reported for similar Eu(III) complexes, [Eu(fod)<sub>3</sub>(tppo)<sub>2</sub>] (0.710 ms),<sup>49</sup> [Eu(fod)<sub>3</sub>(impy)] (0.790 ms),<sup>50</sup> [Eu(fod)<sub>3</sub>(μ-bpp)Eu(fod)<sub>3</sub>] (0.710 ms)<sup>51</sup> and [Eu(fod)<sub>3</sub>(py-im)] (0.798 ms),<sup>52</sup> but longer than [Eu(dbm)<sub>3</sub>(impy)] (0.420 ms),<sup>53</sup> [Eu(tta)<sub>3</sub>(Ph)] (0.092 ms),<sup>54</sup> [Eu(tta)<sub>3</sub>(NP)] (0.084 ms),<sup>54</sup> [Eu(tmh)<sub>3</sub>(py)<sub>2</sub>] (0.510 ms),<sup>55</sup> [Eu(tta)<sub>3</sub>(TPA)] (0.070 ms),<sup>54</sup> [Eu(fod)<sub>3</sub>(bzi)] (0.346 ms)<sup>52</sup> and [Eu(fod)<sub>3</sub>(bath)] (0.799 ms).<sup>52</sup> This result indicates that the antenna effect is highly efficient in the present ternary Eu(III) complexes.<sup>56</sup>

**5.5.5 Color fine tuning.** Chromaticity coordinates defined by the Commission Internationale de l'Éclairage (CIE) provide valuable insight into the color purity and visual perception of emitted light from photoluminescent materials.<sup>57</sup> CIE values of prepared complexes were assessed from their PL emission spectra recorded in the solution state. These results demonstrate the potential of modulation in ligand structure and its coordination mode in fine tuning emission properties (Fig. 8). Through deliberate molecular engineering such as altering substituents or functionalizing the ligand backbone it becomes feasible to design single molecular systems capable of emitting across the visible spectrum, including white light. The synthesized complexes exhibit intense red luminescence with CIE

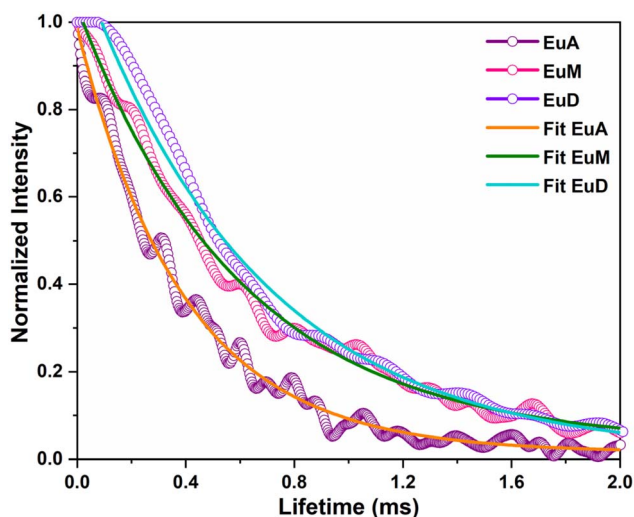


Fig. 7 Decay time profiles of EuA–EuD.



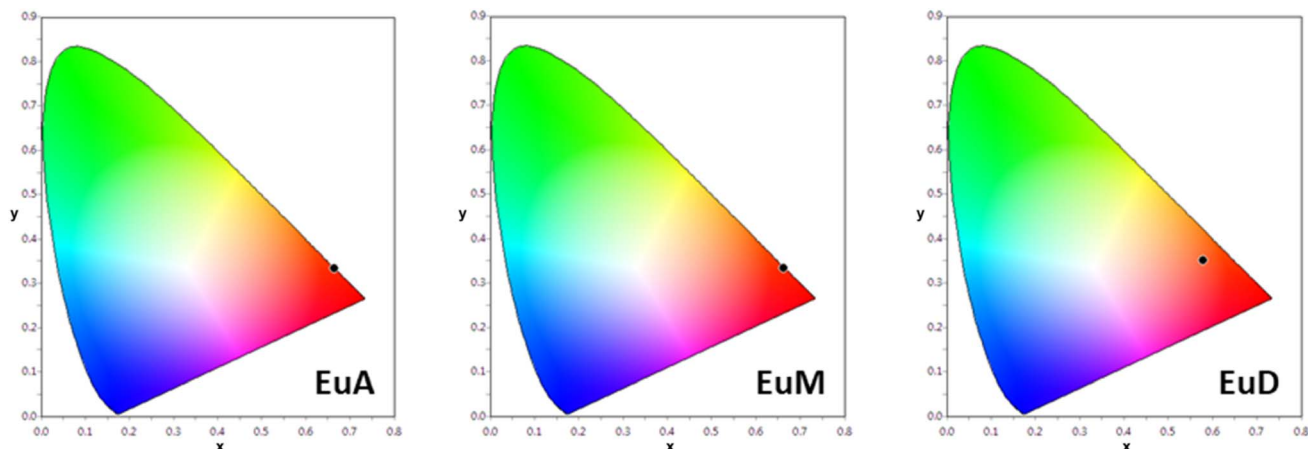


Fig. 8 (x, y) Coordinates of EuA–EuD in DCM.

chromaticity coordinates closely aligned with the pure red emission standard defined by the National Television System Committee (NTSC), which specifies values around ( $x = 0.67$ ;  $y = 0.33$ ).<sup>58</sup> These emissions exhibit remarkably narrow FWHM values of 9.31 nm (EuA), 8.59 nm (EuM) and 9.34 nm (EuD) (Table 7), further indicates their highly monochromatic nature. The determined CIE color coordinates are compiled in Table 7, which are nearly identical to NTSC standard for pure red emission. This monochromaticity in color and spectral sharpness suggest that these Eu(III) based complexes are excellent candidates for application as red emitters in various electroluminescent (EL) and other photonic devices. In summary, the results of the CIE analysis, PL spectral features and structural evaluations confirm that prepared complexes emit bright, spectrally pure red light with high color reliability. The combination of narrow band emission, high intensity ratio and CIE coordinates matching the NTSC red standard makes these materials promising candidates for incorporation into red emitting components in advanced photonic and optoelectronic applications.<sup>59</sup> Ongoing efforts in our laboratory aim to further optimize ligand architectures to achieve broader color tunability, including near white light emission, thus expanding their potential use in full color display technologies and solid state lighting systems.  $u'$  and  $v'$  data was determined by replacing the corresponding  $x$ ,  $y$  data into eqn (5).<sup>60</sup> Obtained points have been plotted in CIE 1976 color chart (Fig. S7, SI).

$$u' = \frac{4x}{-2x + 12y + 3}, \quad v' = \frac{9y}{-2x + 12y + 3} \quad (5)$$

Table 7 Colorimetric data of EuA–EuD

Complex	EuA	EuM	EuD
$x, y$	0.664, 0.334	0.663, 0.332	0.578, 0.350
$u', v'$	0.468, 0.529	0.468, 0.528	0.382, 0.521
CCT	3310	3346	1848
FWHM	9.31	8.59	9.34

Analysis of quality of emitted light produced from prepared complexes was made using McCamy relation of correlated color temperature (CCT) by eqn (6).<sup>61</sup>

$$\text{CCT} = -437n^3 + 3601n^2 - 6861n + 5514.31 \quad (6)$$

In eqn (6),  $n$  is reciprocal slope and is given by  $\frac{(x - x_e)}{(y - y_e)}$ . CCT values for prepared complexes are concised in Table 7. Measured CCT values for the prepared complexes (below 3500 K) in solution indicate emission within the red light region, closely resembling color of fireplace.<sup>62</sup> This makes them ideal for lighting solutions in cozy and intimate environments where natural light like luminescence is preferred. Based on this criterion, these complexes demonstrate strong potential as warm red light sources for practical lighting applications.<sup>63</sup>

**5.5.6 Judd–Ofelt calculation.** Judd–Ofelt (J–O) theory provides a fundamental framework for evaluating photophysical behavior of lanthanide complexes, particularly in elucidating the nature of coordination surrounding of Eu(III) ion. The J–O intensity parameters, specifically  $\Omega_2$  and  $\Omega_4$ , are instrumental in interpreting the degree of asymmetry and covalent or ionic character of bonding interactions between Eu(III) ion and its coordinating ligands. These parameters serve as the foundation for quantifying sensitization efficiency and calculating additional optical features of Eu(III) based complexes.  $\Omega_2$  and  $\Omega_4$  for prepared complexes were derived from their PL emission spectra using the following relationship (eqn (7)):<sup>64</sup>

$$\Omega_\lambda = \frac{D_{\text{MD}} \bar{\nu}^3}{e^2 \bar{\nu}_\lambda^3 U^\lambda} \frac{9n_1^3}{n_\lambda(n_\lambda^2 + 2)^2} \frac{J_\lambda}{J_1} \quad (7)$$

In this equation,  $\nu$  and  $\nu_\lambda$  represent average wavenumbers (in  $\text{cm}^{-1}$ ) for MD and ED transition ( $\Delta J = \lambda$ ), respectively. The parameter  $D_{\text{MD}}$ , denoting the oscillator strength for the magnetic dipole transition ( $\Delta J = 1$ ), is treated as a constant ( $9.6 \times 10^{42}$  esu  $\text{cm}^2$ ) due to its insensitivity to the local bonding environment. This reference value is used for calibrating the oscillator strengths of other electric dipole transitions.  $n$



denotes refractive index of medium and  $e$  is elementary charge ( $4.8 \times 10^{-10}$  esu). The term  $U_\lambda$  represents the squared reduced matrix element  $|J|U_\lambda|J'|^2$ , with values typically ranging from 0 to 0.0032 ( $\Delta J = 2$ ) and 0.0023 ( $\Delta J = 4$ ). Due to the absence of the  $\Delta J = 6$  transition in the recorded emission spectra,  $\Omega_6$  could not be determined. The magnitude of  $\Omega_2$  is especially significant, as it correlates with the asymmetry and polarizability of the coordination sphere around the Eu(III) ion. Larger  $\Omega_2$  values indicate a more distorted, low symmetry environment, which enhances the electric dipole transition probability. Conversely, the  $\Omega_4$  parameter, though still informative, is less sensitive to symmetry variations and is more reflective of the rigidity and compactness of the surrounding ligand field. Therefore, distinct variations in  $\Omega_2$  can be directly attributed to changes in the coordination environment of Eu(III) ions across different complexes. The  ${}^5D_0 \rightarrow {}^7F_1$  transition, governed purely by MD character ( $\Delta J = 1$ ), is largely unaffected by surrounding thus, serves as an internal reference for determining intensity parameters of the ED transitions. Oscillator strengths  $D_{\varepsilon D}^\lambda$  of ED transitions ( $\Delta J = 2$  and 4) were subsequently calculated using eqn (8):<sup>65</sup>

$$D_{\varepsilon D}^\lambda = e^2 \Omega_\lambda U^\lambda \quad (8)$$

Using these values, the radiative transition probabilities  $A_\lambda$  for each emission line were estimated via eqn (9):<sup>66</sup>

$$A_\lambda = \frac{64\pi^4 \tilde{\nu}_\lambda^3 n_\lambda (n_\lambda^2 + 2)^2}{3h} D_{\varepsilon D}^\lambda \quad (9)$$

As per selection rules for f-f transitions,  $\Delta J = 0, \pm 1$  transitions are allowed for MD processes, while  $\Delta J = 2, 4, 6$  are allowed for electric dipole processes. Transitions such as  $\Delta J = 0, 3$  and 5 are forbidden and as expected, their corresponding  $A_\lambda$  values were calculated to be zero. For the magnetic dipole transition ( $\Delta J = 1$ ), the equation simplifies to eqn (10):

$$A_1 = \frac{64\pi^4 \tilde{\nu}_1^3}{3h} n_1^3 D_{MD} \quad (10)$$

The obtained radiative transition rates were further used to compute the branching ratios ( $\beta_R$ ) for each transition using eqn (11).<sup>66</sup> Branching ratio is a vital parameter in laser material design, as it defines the likelihood of photon emission from a specific transition, relative to the total emission probability. A higher  $\beta_R$  indicates a greater contribution to stimulated emission and an enhanced potential for achieving laser amplification. The calculated  $\beta_R$  for the prepared complexes are tabulated in Table 9. The  $\beta_R$  values follow the order:  ${}^5D_0 \rightarrow {}^7F_2 > {}^5D_0 \rightarrow {}^7F_4 > {}^5D_0 \rightarrow {}^7F_1$ , with the  ${}^5D_0 \rightarrow {}^7F_2$  transition exhibiting the highest contribution (approximately 85%) to total emission. This dominance makes it the most favorable transition for optical amplification and laser design purposes.

$$\beta = \frac{A_{0-J}}{\sum_{J=1,2,4} A_{0-J}} \quad (11)$$

Table 8 Several theoretical structural parameters of EuA–EuD

Complex	Asymmetry ratio		$\Omega_2 (\times 10^{-20} \text{ cm}^2)$		$\Omega_4 (\times 10^{-20} \text{ cm}^2)$	
	Exp. (theo.)	Exp.	Theo.	Exp.	Theo.	
EuA	15.28 (15.79)	19.106	16.064	5.642	5.627	
EuM	18.19 (13.77)	19.687	16.672	4.819	2.262	
EuD	3.26 (3.07)	4.090	5.640	3.665	3.965	

Table 9  $\beta_R$  and  $A_\lambda$  of characteristic peaks in EuA–EuD (solution)<sup>a</sup>

Complex	EuA	EuM	EuD
$\beta ({}^5D_0 \rightarrow {}^7F_1)$	0.056 (0.054)	0.047 (0.063)	0.210 (0.219)
$\beta ({}^5D_0 \rightarrow {}^7F_2)$	0.856 (0.853)	0.855 (0.868)	0.686 (0.673)
$\beta ({}^5D_0 \rightarrow {}^7F_4)$	0.087 (0.093)	0.096 (0.069)	0.103 (0.108)
$A_\lambda ({}^5D_0 \rightarrow {}^7F_1)$	115.679	115.691	113.283
$A_\lambda ({}^5D_0 \rightarrow {}^7F_2)$	1529.194	1576.039	327.331
$A_\lambda ({}^5D_0 \rightarrow {}^7F_4)$	176.534	189.029	192.822

<sup>a</sup> ( ) contains theoretical values.

The experimental photophysical parameters demonstrated excellent agreement with theoretical predictions calculated using the JOES software package. The complete set of evaluated Judd–Ofelt parameters, radiative rates, oscillator strengths and branching ratios is summarized in Tables 8 and 9, further validating the high quality optical performance of the synthesized Eu(III) complexes.

## 5.6 Thermal analysis

Thermal stability is a key factor influencing the applicability of lanthanide based complexes in OLED technologies.<sup>67</sup> To assess this, the thermal behavior of both mononuclear (binary and ternary) and dinuclear europium complexes was analyzed using thermogravimetric analysis (TGA) under a nitrogen atmosphere. The weight loss patterns of EuM and EuD are depicted in Fig. S8 (in SI). For EuA, the TGA profile shows a two step weight loss pattern. First step appears near 100 °C and corresponds to release of two coordinated water molecules. This indicates that only TTBD remain bonded to Eu(III) center beyond this temperature. The thermogravimetric analysis (TGA) curve of EuM reveals a total mass loss of 83.43% (calculated 83.58%) over the temperature range of 169 °C to 534 °C. The initial, minor weight loss of approximately 15.24% (theoretical 15.27%) observed between 169 °C and 339 °C is due to release of pyz units. A major decomposition phase occurs around 458 °C, causing a significant mass-loss of 65.04% (theoretical 68.31%), ascribed to detachment of the TTBD ligands, with this degradation till 534 °C. The final decomposition residue, based on mass loss calculations, is identified as europium oxide (Eu<sub>2</sub>O<sub>3</sub>).

TGA profile of the dinuclear complex reveals an initial weight loss of approximately 50.18% occurring around 225 °C and 359 °C (residual mass: 47.65%). This step is associated with the degradation of the TTBD ligands. A subsequent major degradation step is observed at 463 °C (with a 22% loss), corresponding to



the breakdown of the bridging pyz moiety. Final decomposition events take place at higher temperature (547 °C) indicating the thermal stability of complex. When compared with its mononuclear counterparts, the dinuclear Eu(III) complex incorporating a spacer ligand demonstrates significantly enhanced thermal resistance. Among the mononuclear species, the binary complex shows the lowest thermal stability, primarily due to presence of coordinated water molecules, which begin to decompose at temperatures as low as 100 °C.

### 5.7 Computational modeling

Electronic structures of the complexes were determined using Density Functional Theory (DFT) calculations at def2-SVP basis

set level,<sup>68</sup> implemented through ORCA 5.0.4 software.<sup>69</sup> Initial three dimensional molecular models were constructed and optimized using Avogadro.<sup>70</sup> Final geometry optimizations were carried out *via* DFT and the optimized structures are displayed in Table 10. These optimized geometries served as the basis for calculating energies of highest occupied molecular orbital (HOMO) and lowest unoccupied molecular orbital (LUMO) using time dependent DFT (TDDFT), conducted in ORCA 5.0.4. To account for relativistic effects in lanthanide atoms, a large core quasi relativistic effective core potential was applied alongside the basis set. For EuA–EuD, the calculated HOMO and LUMO energies are summarized in Table 10 along with their corresponding frontier molecular orbital (FMO) diagrams.

Table 10 Structure and energy levels (in eV) of EuA–EuD

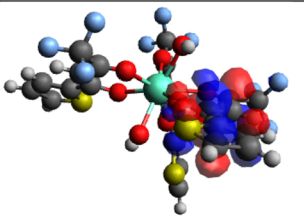
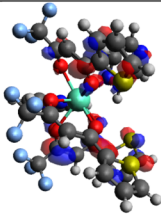
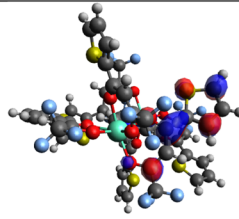
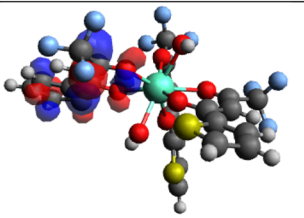
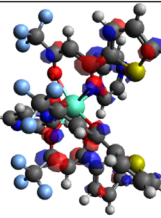
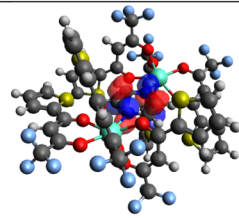
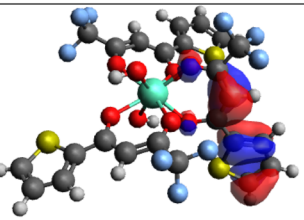
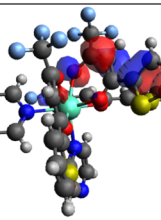
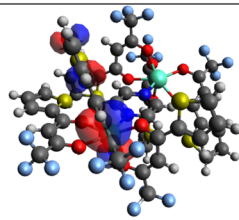
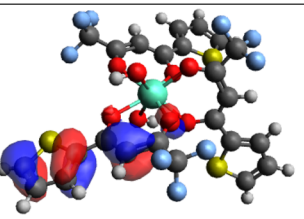
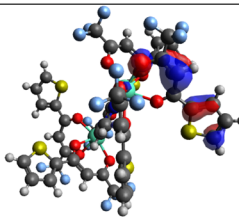
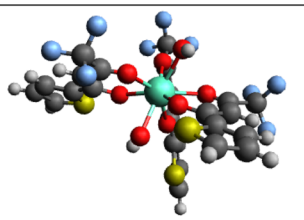
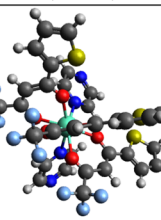
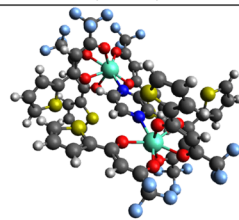
LUMO + 1	 (-2.011)	 (-1.689)	 (-1.461)
LUMO	 (-3.224)	 (-3.350)	 (-3.427)
HOMO	 (-6.517)	 (-6.623)	 (-6.668)
HOMO - 1	 (-7.211)	 (-7.479)	 (-7.552)
Complex	 EuA	 EuM	 EuD



Table 11 Molecular parameters of prepared complexes

Complex	Bandgap	IE	EA	$\chi$	$\eta$	$\sigma$	$\mu$
EuA	3.293	6.517	3.224	4.870	1.646	0.607	-4.870
EuM	3.273	6.623	3.350	4.986	1.636	0.611	-4.986
EuD	3.241	6.668	3.427	5.047	1.620	0.617	-5.047

The calculated band gaps are compiled in Table 11. With band gap values in the range of 3–4 eV, these complexes show potential for optoelectronic applications. Using Koopmans' theorem (eqn (12)), the Ionization Energy (IE) and Electron Affinity (EA) were derived from HOMO and LUMO energy levels.<sup>71</sup> Various global reactivity descriptors were calculated, including chemical hardness ( $\eta$ ), chemical potential ( $\mu$ ), electron affinity ( $\chi$ ), softness ( $\sigma$ ) and Fukui functions, as shown in eqn (13).<sup>72</sup> These parameters, detailed in Table 11, offer insights into chemical reactivity and stability complexes. Thus, help to predict reactive sites, estimate reaction rates and evaluate susceptibility to side reactions thereby helping in the rational design and optimization of chemical processes.

$$IE = -E_{\text{HOMO}}, EA = -E_{\text{LUMO}} \quad (12)$$

$$\chi = \frac{IE + EA}{2}, \eta = \frac{IE - EA}{2}, \sigma = \frac{1}{\eta}, \mu = -\chi \quad (13)$$

## 6. Conclusions

Single component red emissive luminescent materials with strong emission properties are highly promising as color converters in LED applications. In this regard, a thiophene-based  $\beta$ -diketone ligand, 4,4,4-trifluoro-1-(2-thienyl)-1,3-butanedione (TTBD), bearing a trifluorobutane group in the opposing position, was utilized to construct a dinuclear Eu(III) ternary complex, [Eu<sub>2</sub>(TTBD)<sub>6</sub>pyz] (EuD), where pyz refers to pyrazine. Additionally, a mononuclear counterpart (EuM) and a binary analogue (EuA) were also synthesized. Comprehensive characterization of these complexes was performed using IR, NMR, UV-vis, PL, time resolved spectroscopy and TGA. Dinuclear Eu(III) complexes demonstrated excellent thermal stability and broad, intense excitation bands ranging from 200–350 nm (monitored at 612 nm). Under near UV excitation, it exhibited strong red luminescence, attributed to the f-f transitions of the Eu(III) ion. Importantly, the luminescence of the dinuclear complex significantly outperformed its mononuclear analogues, indicating cooperative enhancement from both europium centers. The absence of ligand centered emission further confirms effective energy transfer from ligand to metal ion. Based on its emission spectrum, CIE chromaticity coordinates ( $x = 0.66$ ,  $y = 0.33$ ) validate its suitability as a red phosphor for white LED applications. Fluorescence lifetime measurements and the triplet state energy level of TTBD (20 600 cm<sup>-1</sup>), which exceeds energy of Eu(III) <sup>5</sup>D<sub>0</sub> excited state, confirm a ligand sensitized (antenna effect) luminescence mechanism. This conclusion is supported by both Judd–Ofelt (JOES) theoretical analysis and density functional theory (DFT)

computations, which also elucidated the electronic density distribution within the complexes. Overall, these findings highlight the practical potential of the synthesized europium complexes as efficient red components in near UV excited white light emitting diodes.

## Author contributions

Vandana Aggarwal = data curation, writing – original draft; Devender Singh = writing – review & editing and supervision; Sofia Malik = investigation; Shri Bhagwan = visualization; Sumit Kumar = resources; Rajender Singh Malik = validation; Parvin Kumar = software; Jayant Sindhu = formal analysis.

## Conflicts of interest

There are no conflicts to declare.

## Data availability

The authors affirm that the information/data of this research article is available inside the article.

Supplementary information is available. See DOI: <https://doi.org/10.1039/d5ra06968h>.

## Acknowledgements

Vandana Aggarwal is thankful to UGC-New Delhi for providing JRF [221610012377].

## References

- V. Aggarwal, D. Singh, A. Hooda, S. Malik, S. Dalal, S. Redhu, S. Kumar, R. S. Malik and P. Kumar, Comprehensive investigation of ternary dysprosium complexes for white light emission: Synthesis, spectroscopic and colorimetric analyses, *J. Lumin.*, 2024, **270**, 120555, DOI: [10.1016/j.jlumin.2024.120555](https://doi.org/10.1016/j.jlumin.2024.120555).
- M. L. Reddy and K. S. Bejoymohandas, Luminescent lanthanide-based molecular materials: applications in photodynamic therapy, *Dalton Trans.*, 2024, **53**, 1898–1914, DOI: [10.1039/D3DT04064J](https://doi.org/10.1039/D3DT04064J).
- M. L. Reddy, K. S. Bejoymohandas and V. Divya, Luminescent lanthanide coordination compounds as potential mitochondria-targeting probes: Molecular engineering to bioimaging, *Dyes Pigm.*, 2022, **205**, 110528, DOI: [10.1016/j.dyepig.2022.110528](https://doi.org/10.1016/j.dyepig.2022.110528).
- V. Aggarwal, D. Singh, A. Hooda, K. Nehra, S. Kumar, R. S. Malik and P. Kumar, Synthesis and photoluminescent analyses of ternary terbium (III) Tris- $\beta$ -diketonate complexes: A systematic exploration, *J. Mater. Sci. Mater. Electron.*, 2024, **25**, 568, DOI: [10.1007/s10854-024-12314-z](https://doi.org/10.1007/s10854-024-12314-z).
- S. I. Weissman, Intramolecular energy transfer the fluorescence of complexes of europium, *J. Chem. Phys.*, 1942, **10**, 214–217, DOI: [10.1063/1.1723709](https://doi.org/10.1063/1.1723709).
- M. Latva, H. Takalo, V. M. Mukkala, C. Matachescu, J. C. Rodríguez-Ubis and J. Kankare, Correlation between



- the lowest triplet state energy level of the ligand and lanthanide(III) luminescence quantum yield, *J. Lumin.*, 1997, **75**, 149–169, DOI: [10.1016/S0022-2313\(97\)00113-0](https://doi.org/10.1016/S0022-2313(97)00113-0).
- 7 V. Aggarwal, D. Singh, S. Bhagwan, R. K. Saini, K. Jakhar, S. Kumar, P. Kumar and J. Sindhu, Tuning emissive color of trivalent terbium ion through environmental factors: optoelectronic insights from theoretical, spectral and computational studies, *RSC Adv.*, 2024, **14**, 39569–39587, DOI: [10.1039/D4RA05334F](https://doi.org/10.1039/D4RA05334F).
- 8 C. Q. Shen, T. L. Yan, Y. T. Wang, Z. J. Ye, C. J. Xu and W. J. Zhou, Synthesis, structure and luminescence properties of binary and ternary complexes of lanthanide ( $\text{Eu}^{3+}$ ,  $\text{Sm}^{3+}$  and  $\text{Tb}^{3+}$ ) with salicylic acid and 1,10-phenanthroline, *J. Lumin.*, 2017, **184**, 48–54, DOI: [10.1016/j.jlumin.2016.12.018](https://doi.org/10.1016/j.jlumin.2016.12.018).
- 9 S. A. Ansari, L. Liu and L. Rao, Binary lanthanide(III)/nitrate and ternary lanthanide(III)/nitrate/chloride complexes in an ionic liquid containing water: optical absorption and luminescence studies, *Dalton Trans.*, 2015, **44**, 2907–2914, DOI: [10.1039/C4DT03479A](https://doi.org/10.1039/C4DT03479A).
- 10 M. A. Guino-o, B. Bustrom, R. A. Tigaa and A. de Bettencourt-Dias, Microwave-assisted synthesis of ternary lanthanide (2-thenoyltrifluoroacetone)<sub>3</sub>(triphenylphosphine oxide)<sub>2</sub> complexes, *Inorg. Chim. Acta*, 2017, **464**, 23–30, DOI: [10.1016/j.ica.2017.04.021](https://doi.org/10.1016/j.ica.2017.04.021).
- 11 K. Nehra, A. Dalal, A. Hooda, D. Singh, S. Kumar and R. S. Malik, Heteroleptic luminous ternary europium Complexes: Synthesis, electrochemical and photophysical investigation, *Chem. Phys. Lett.*, 2022, **800**, 139675, DOI: [10.1016/j.cplett.2022.139675](https://doi.org/10.1016/j.cplett.2022.139675).
- 12 Q. Zhou, F. Yang, D. Liu, Y. Peng, G. Li, Z. Shi and S. Feng, Synthesis, structures, and magnetic properties of three fluoride-bridged lanthanide compounds: effect of bridging fluoride ions on magnetic behaviors, *Inorg. Chem.*, 2012, **51**, 7529–7536, DOI: [10.1021/ic300125y](https://doi.org/10.1021/ic300125y).
- 13 W. K. Wong, X. Zhu and W. Y. Wong, Synthesis, structure, reactivity and photoluminescence of lanthanide(III) monoporphyrinate complexes, *Coord. Chem. Rev.*, 2007, **251**, 2386–2399, DOI: [10.1016/j.ccr.2006.11.014](https://doi.org/10.1016/j.ccr.2006.11.014).
- 14 G. Li, D. Zhu, X. Wang, Z. Su and M. R. Bryce, Dinuclear metal complexes: multifunctional properties and applications, *Chem. Soc. Rev.*, 2020, **49**, 765–838, DOI: [10.1039/C8CS00660A](https://doi.org/10.1039/C8CS00660A).
- 15 G. Qian-Ling, Z. Wen-Xiang, G. Rong, Y. Xi and W. Ru-Ji, Crystal Structure of Complex Tris(4,4,4-trifluoro-1-phenyl-1,3-butanedione)(1,10-phenanthroline) Europium(III), *Chin. J. Chem.*, 2003, **21**, 211–215, DOI: [10.1002/cjoc.20030210225](https://doi.org/10.1002/cjoc.20030210225).
- 16 M. O. Yusuf, Bond characterization in cementitious material binders using Fourier-transform infrared spectroscopy, *Appl. Sci.*, 2023, **13**, 3353, DOI: [10.3390/app13053353](https://doi.org/10.3390/app13053353).
- 17 A. Dalal, K. Nehra, A. Hooda, D. Singh, J. Dhankhar and S. Kumar, Fluorinated  $\beta$ -diketone-based Sm(III) complexes: spectroscopic and optoelectronic characteristics, *Luminescence*, 2022, **37**, 1328–1334, DOI: [10.1002/bio.4300](https://doi.org/10.1002/bio.4300).
- 18 M. S. Ansari and N. Ahmad, Studies on the mixed ligand complexes of rare earths with dipivaloylmethane and pyrazine, *J. Inorg. Nucl. Chem.*, 1975, **37**, 2099–2101, DOI: [10.1016/0022-1902\(75\)80838-4](https://doi.org/10.1016/0022-1902(75)80838-4).
- 19 K. Iftikhar, A. U. Malik and N. Ahmad, *J. Chem. Soc., Dalton Trans.*, 1985, 2547–2550, DOI: [10.1039/dt9850002547](https://doi.org/10.1039/dt9850002547).
- 20 R. Ilmi and K. Iftikhar, Pyrazine bridged Ln<sub>2</sub> (La, Nd, Eu and Tb) complexes containing fluorinated  $\beta$ -diketone, *Inorg. Chem. Commun.*, 2012, **20**, 7–12, DOI: [10.1016/j.inoche.2012.01.037](https://doi.org/10.1016/j.inoche.2012.01.037).
- 21 V. Aggarwal, D. Singh, K. Nehra, S. Dalal, S. Redhu, P. Kumar, S. Kumar and R. S. Malik, White light emission from a ternary dysprosium complex: Energy transfer and ligand-driven modulation, *Mater. Sci. Semicond. Process.*, 2025, **192**, 109427, DOI: [10.1016/j.mssp.2025.109427](https://doi.org/10.1016/j.mssp.2025.109427).
- 22 V. Aggarwal, D. Singh, S. Redhu, S. Malik, S. Dalal, S. Kumar, R. S. Malik, P. Kumar and J. Sindhu, Design and photophysical characterization of dinuclear lanthanide complexes incorporating spacer ligands along with their mononuclear analogues: A comparative study, *Opt. Mater.*, 2024, **155**, 115833, DOI: [10.1016/j.optmat.2024.115833](https://doi.org/10.1016/j.optmat.2024.115833).
- 23 V. Aggarwal, D. Singh, A. Hooda, K. Nehra, S. Redhu, S. Kumar, R. S. Malik and P. Kumar, Design and spectroscopic study of samarium complexes with tunable photoluminescent properties, *J. Mol. Struct.*, 2024, **1311**, 138315, DOI: [10.1016/j.molstruc.2024.138315](https://doi.org/10.1016/j.molstruc.2024.138315).
- 24 R. Boddula and S. Vaidyanathan, Bi-nuclear luminescent europium(III) molecular complexes for white light emitting diodes: Experimental and theoretical study, *Inorg. Chim. Acta*, 2019, **494**, 141–153, DOI: [10.1016/j.ica.2019.05.014](https://doi.org/10.1016/j.ica.2019.05.014).
- 25 A. Dolgonos, T. O. Mason and K. R. Poeppelmeier, Direct optical band gap measurement in polycrystalline semiconductors: A critical look at the Tauc method, *J. Solid State Chem.*, 2016, **240**, 43–48, DOI: [10.1016/j.jssc.2016.05.010](https://doi.org/10.1016/j.jssc.2016.05.010).
- 26 A. Hooda, K. Nehra, A. Dalal, S. Singh, S. Bhagwan, K. Jakhar and D. Singh, Preparation and photoluminescent analysis of Sm<sup>3+</sup> complexes based on unsymmetrical conjugated chromophoric ligand, *J. Mater. Sci.: Mater. Electron.*, 2022, **33**, 11132–11142, DOI: [10.1007/s10854-022-08089-w](https://doi.org/10.1007/s10854-022-08089-w).
- 27 K. Binnemans, Interpretation of europium(III) spectra, *Coord. Chem. Rev.*, 2015, **295**, 1–45, DOI: [10.1016/j.ccr.2015.02.015](https://doi.org/10.1016/j.ccr.2015.02.015).
- 28 S. K. Tamang, G. Gurung, R. K. Parajuli, B. Yupeng, K. Neupane, M. J. Kipper, L. A. Belfiore and J. Tang, Smart sensing property of Eu<sup>3+</sup>-induced polyelectrolyte nanoaggregates on nitrofurantoin antibiotics in aqueous environments, *J. Environ. Chem. Eng.*, 2024, **12**, 114145, DOI: [10.1016/j.jece.2024.114145](https://doi.org/10.1016/j.jece.2024.114145).
- 29 L. Blois, A. N. Neto, R. L. Longo, I. F. Costa, T. B. Paolini, H. F. Brito and O. L. Malta, On the experimental determination of 4f-4f intensity parameters from the emission spectra of europium(III) compounds, *Opt. Spectrosc.*, 2022, **130**, 10–17, DOI: [10.1134/S0030400X2201009X](https://doi.org/10.1134/S0030400X2201009X).
- 30 E. H. Hasabeldaim, Luminescence properties of ZnO and ZnO: Eu<sup>3+</sup> nanostructures and thin films, Doctoral dissertation, University of the Free State, 2019, <http://hdl.handle.net/11660/10947>.



- 31 D. Singh and P. Poddar, Tuning the electric dipole transitions ( $^5D_0 \rightarrow ^7F_2$ , and  $^5D_0 \rightarrow ^7F_4$ ) in thin Eu-doped BiOCl nanosheets, *ChemRxiv*, 2025, preprint, DOI: [10.26434/chemrxiv-2025-8q8jd](https://doi.org/10.26434/chemrxiv-2025-8q8jd).
- 32 V. Aggarwal, D. Singh, S. Bhagwan, R. K. Saini, K. Jakhar, R. S. Malik, P. Kumar and J. Sindhu, Exploring the influence of emissive centers in mono and dinuclear europium (III) complexes for advance lighting applications: Synthesis, characterization and computational modeling, *J. Mol. Struct.*, 2025, **1324**, 140841, DOI: [10.1016/j.molstruc.2024.140841](https://doi.org/10.1016/j.molstruc.2024.140841).
- 33 W. M. Wang, H. X. Zhang, S. Y. Wang, H. Y. Shen, H. L. Gao, J. Z. Cui and B. Zhao, Ligand field affected Single-Molecule Magnet behavior of lanthanide(III) dinuclear complexes with an 8-hydroxyquinoline Schiff base derivative as bridging ligand, *Inorg. Chem.*, 2015, **54**, 10610–10622, DOI: [10.1021/acs.inorgchem.5b01404](https://doi.org/10.1021/acs.inorgchem.5b01404).
- 34 V. Aggarwal, D. Singh, A. Hooda, K. Nehra, S. Redhu, S. Kumar, R. S. Malik and P. Kumar, Design and spectroscopic study of samarium complexes with tunable photoluminescent properties, *J. Mol. Struct.*, 2024, **1311**, 138315, DOI: [10.1016/j.molstruc.2024.138315](https://doi.org/10.1016/j.molstruc.2024.138315).
- 35 A. Dalal, K. Nehra, A. Hooda, D. Singh, S. Kumar and R. S. Malik, Red emissive ternary europium complexes: synthesis, optical, and luminescence characteristics, *Luminescence*, 2022, **37**, 1309–1320, DOI: [10.1002/bio.4297](https://doi.org/10.1002/bio.4297).
- 36 W. A. Dar, Z. Ahmed and K. Iftikhar, Cool white light emission from the yellow and blue emission bands of the Dy(III) complex under UV-excitation, *J. Photochem. Photobiol., A*, 2018, **356**, 502–511, DOI: [10.1016/j.jphotochem.2017.12.017](https://doi.org/10.1016/j.jphotochem.2017.12.017).
- 37 Z. Ahmed and K. Iftikhar, Efficient layers of emitting ternary lanthanide complexes for fabricating red, green, and yellow OLEDs, *Inorg. Chem.*, 2015, **54**, 11209–11225, DOI: [10.1021/acs.inorgchem.5b01630](https://doi.org/10.1021/acs.inorgchem.5b01630).
- 38 V. Divya and M. L. Reddy, Visible-light excited red emitting luminescent nanocomposites derived from  $\text{Eu}^{3+}$ -phenanthrene-based fluorinated  $\beta$ -diketonate complexes and multi-walled carbon nanotubes, *J. Mater. Chem. C*, 2013, **1**, 160–170, DOI: [10.1039/C2TC00186A](https://doi.org/10.1039/C2TC00186A).
- 39 S. A. Bhat and K. Iftikhar, Synthesis, characterization, photoluminescence and intensity parameters of high quantum efficiency pure-red emitting Eu(III) fluorinated  $\beta$ -diketonate complexes, *New J. Chem.*, 2019, **43**, 13162–13172, DOI: [10.1039/C9NJ00697D](https://doi.org/10.1039/C9NJ00697D).
- 40 D. Parker, J. D. Fradgley, M. Delbianco, M. Starck, J. W. Walton and J. M. Zwier, Comparative analysis of lanthanide excited state quenching by electronic energy and electron transfer processes, *Faraday Discuss.*, 2022, **234**, 159–174, DOI: [10.1039/D1FD00059D](https://doi.org/10.1039/D1FD00059D).
- 41 K. F. Wong, B. Bagchi and P. J. Rossky, Distance and orientation dependence of excitation transfer rates in conjugated systems: beyond the Förster theory, *J. Phys. Chem. A*, 2004, **108**, 5752–5763, DOI: [10.1021/jp037724s](https://doi.org/10.1021/jp037724s).
- 42 S. Yabu, H. Sato and M. Higashi, Theoretical aspects of Dexter-type excitation energy transfer for understanding optical phenomena on photosynthetic systems, *Chem. Phys. Rev.*, 2025, **6**, DOI: [10.1063/5.0251172](https://doi.org/10.1063/5.0251172).
- 43 M. Kang, X. Liao, Y. Kang, J. Liu, R. Sun, G. Yin, Z. Huang and Y. Yao, Preparation and properties of red phosphor  $\text{CaO:Eu}^{3+}$ , *J. Mater. Sci.*, 2009, **44**, 2388–2392, DOI: [10.1007/s10853-009-3298-x](https://doi.org/10.1007/s10853-009-3298-x).
- 44 H. Li, L. Liu, G. Fu, B. Li, X. Lü, W. K. Wong and R. A. Jones, Pure white-light and color-tuning of PMMA-supported hybrid materials doped with  $(\text{TTA})_3\text{-Zn}^{2+}\text{-Eu}^{3+}$  and  $(\text{BA})_3\text{-Zn}^{2+}\text{-Tb}^{3+}$  complexes, *Inorg. Chem. Commun.*, 2016, **72**, 54–56, DOI: [10.1016/j.inoche.2016.08.004](https://doi.org/10.1016/j.inoche.2016.08.004).
- 45 Y. Hidalgo-Rosa, J. Santoyo-Flores, M. A. Treto-Suárez, E. Schott, D. Pérez-Hernández and X. Zarate, Tuning the sensitization pathway  $T_1 \rightarrow ^5D_J$  in Eu-based MOF through modification of the antenna ligand. A theoretical approach via multiconfigurational quantum calculations, *J. Lumin.*, 2023, **260**, 119896, DOI: [10.1016/j.jlumin.2023.119896](https://doi.org/10.1016/j.jlumin.2023.119896).
- 46 J. Shi, F. Tian, J. Lyu and M. Yang, Nanoparticle based fluorescence resonance energy transfer (FRET) for biosensing applications, *J. Mater. Chem. B*, 2015, **3**, 6989–7005, DOI: [10.1039/C5TB00885A](https://doi.org/10.1039/C5TB00885A).
- 47 J. Chen, J. Lv, X. Liu, J. Lin and X. Chen, A study on theoretical models for investigating time-resolved photoluminescence in halide perovskites, *Phys. Chem. Chem. Phys.*, 2023, **25**, 7574–7588, DOI: [10.1039/D2CP05723A](https://doi.org/10.1039/D2CP05723A).
- 48 K. Nehra, A. Dalal, A. Hooda, P. Kumar, D. Singh, S. Kumar, R. S. Malik and P. Kumar, Luminous terbium and samarium complexes with diacetylmethane and substituted 1,10-phenanthroline derivatives for display applications: Preparation and optoelectronic investigations, *J. Lumin.*, 2022, **249**, 119032, DOI: [10.1016/j.jlumin.2022.119032](https://doi.org/10.1016/j.jlumin.2022.119032).
- 49 S. A. Bhat and K. Iftikhar, Optical properties and intensity parameters of UV excited efficient red emitting Europium complexes containing fluorinated 1,3-Dione as primary sensitizer in solution, solid and PMMA thin films, *Opt. Mater.*, 2020, **99**, 109600, DOI: [10.1016/j.optmat.2019.109600](https://doi.org/10.1016/j.optmat.2019.109600).
- 50 S. A. Bhat and K. Iftikhar, Synthesis, characterization, photoluminescence and intensity parameters of high quantum efficiency pure-red emitting Eu(III) fluorinated  $\beta$ -Diketone complexes, *New J. Chem.*, 2019, **43**, 13162–13172, DOI: [10.1039/c9nj00697d](https://doi.org/10.1039/c9nj00697d).
- 51 A. B. Ganaie and K. Iftikhar, Theoretical modeling (sparkle RM1 and PM7) and crystal structures of the luminescent dinuclear Sm(III) and Eu(III) complexes of 6,6,7,7,8,8,8-Heptafluoro-2,2-Dimethyl-3,5-Octanedione and 2,3-Bis(2-Pyridyl)Pyrazine: determination of individual spectroscopic Parameters for Two Unique  $\text{Eu}^{3+}$  Sites, *ACS Omega*, 2021, **6**, 21207–21226, DOI: [10.1021/acsomega.0c05976](https://doi.org/10.1021/acsomega.0c05976).
- 52 A. Ali, Z. Ahmed, N. Rahisuddin and K. Iftikhar, Pure red-light emitting Europium based complexes as efficient UV light converters: synthesis, crystal structure and photoluminescence properties, *Dalton Trans.*, 2023, **52**, 14075–14087, DOI: [10.1039/d3dt01536j](https://doi.org/10.1039/d3dt01536j).
- 53 N. Hasan and K. Iftikhar, Synthesis, Crystal structure and photoluminescence studies of  $[\text{Eu}(\text{dbm})_3(\text{impy})]$  and its



- polymer-based hybrid film, *New J. Chem.*, 2019, **43**, 2479–2489, DOI: [10.1039/c8nj04560g](https://doi.org/10.1039/c8nj04560g).
- 54 K. Singh, R. Boddula and S. Vaidyanathan, Versatile luminescent Europium(III)- $\beta$ -Diketonate-Imidazo-Bipyridyl complexes intended for white LEDs: a detailed photophysical and theoretical study, *Inorg. Chem.*, 2017, **56**, 9376–9390, DOI: [10.1021/acs.inorgchem.7b01565](https://doi.org/10.1021/acs.inorgchem.7b01565).
- 55 P. P. Ferreira Da Rosa, S. Miyazaki, H. Sakamoto, Y. Kitagawa, K. Miyata, T. Akama, M. Kobayashi, K. Fushimi, K. Onda, T. Taketsugu and Y. Hasegawa, Coordination geometrical effect on ligand-to-metal charge transfer-dependent energy transfer processes of luminescent Eu(III) complexes, *J. Phys. Chem. A*, 2021, **125**, 209–217, DOI: [10.1021/acs.jpca.0c09337](https://doi.org/10.1021/acs.jpca.0c09337).
- 56 A. Ali, Z. Ahmed and K. Iftikhar, Homo-dinuclear Samarium<sup>III</sup> and Europium<sup>III</sup> Complexes with remarkable Quantum Yields: Orange-Red and Bright-Red Emitters, *Opt. Mater.*, 2025, 117583, DOI: [10.1016/j.optmat.2025.117583](https://doi.org/10.1016/j.optmat.2025.117583).
- 57 G. Karagiannis and S. Amanatiadis, Colour Measurements and Ultraviolet/Visible Spectroscopy, in *Non-Destructive Methodologies and Adapted Signal Processing Techniques in the Field of Cultural Heritage*, Springer Nature Switzerland, Cham, 2025, pp. 153–183, DOI: [10.1007/978-3-031-85780-5\\_10](https://doi.org/10.1007/978-3-031-85780-5_10).
- 58 P. Arsenyan, A. Petrenko, K. Leitonas, D. Volyniuk, J. Simokaitiene, T. Klinavičius, E. Skuodis, J. H. Lee and J. V. Gražulevičius, Synthesis and performance in OLEDs of selenium-containing phosphorescent emitters with red emission color deeper than the corresponding NTSC standard, *Inorg. Chem.*, 2019, **58**, 10174–10183, DOI: [10.1021/acs.inorgchem.9b01283](https://doi.org/10.1021/acs.inorgchem.9b01283).
- 59 P. Aggarwal, D. Singh, P. Kumar, S. Dalal, S. Kumar, R. S. Malik, P. Kumar, J. Sindhu and H. Kumar, DFT Studies and Experimental Characterization of Eu<sup>3+</sup> Complexes in Different Coordinating Environment: A Comprehensive Approach to Luminescence and Applications in Display Technologies, *J. Mol. Struct.*, 2025, 142781, DOI: [10.1016/j.molstruc.2025.142781](https://doi.org/10.1016/j.molstruc.2025.142781).
- 60 S. Redhu, D. Singh, A. Hooda, A. Dalal, S. Kumar, R. S. Malik, V. Siwach and P. Kumar, Preparation, characterization and spectroscopic analyses of Dy(III)  $\beta$ -diketonates with bidentate N donor neutral ligands for displays, *J. Photochem. Photobiol., A*, 2024, **449**, 115381, DOI: [10.1016/j.jphotochem.2023.115381](https://doi.org/10.1016/j.jphotochem.2023.115381).
- 61 C. S. McCamy, Correlated color temperature as an explicit function of chromaticity coordinates, *Color Res. Appl.*, 1992, **17**, 142–144, DOI: [10.1002/col.5080170211](https://doi.org/10.1002/col.5080170211).
- 62 U. Das, A. Das, M. Islam, R. Das and A. K. Das, Chemistry Behind the Mystery of Colors of Different Objects-Part 1, *Resonance*, 2024, **29**, 1643–1668, DOI: [10.1007/s12045-024-1643-7](https://doi.org/10.1007/s12045-024-1643-7).
- 63 V. Aggarwal, D. Singh, A. Hooda, K. Jakhar, S. Kumar, R. S. Malik and P. Kumar, Optimizing europium (III) ion luminescence via  $\beta$ -diketone and auxiliary ligands: analysis of optoelectronic features and Judd-Ofelt parameters, *Chem. Phys. Lett.*, 2025, 142244, DOI: [10.1016/j.cplett.2025.142244](https://doi.org/10.1016/j.cplett.2025.142244).
- 64 A. Dalal, K. Nehra, A. Hooda, D. Singh, S. Kumar and R. S. Malik, Red emissive ternary europium complexes: synthesis, optical, and luminescence characteristics, *Luminescence*, 2022, **37**, 1309–1320, DOI: [10.1002/bio.4297](https://doi.org/10.1002/bio.4297).
- 65 K. Nehra, A. Dalal, A. Hooda, D. Singh, S. Kumar, R. S. Malik and P. Kumar, Influence of coordinating environment on photophysical properties of UV excited sharp red emitting material: Judd Ofelt analysis, *J. Photochem. Photobiol., A*, 2022, **430**, 113999, DOI: [10.1016/j.jphotochem.2022.113999](https://doi.org/10.1016/j.jphotochem.2022.113999).
- 66 K. Nehra, A. Dalal, A. Hooda, D. Singh, S. Kumar and R. S. Malik, Heteroleptic luminous ternary europium Complexes: Synthesis, electrochemical and photophysical investigation, *Chem. Phys. Lett.*, 2022, **800**, 139675, DOI: [10.1016/j.cplett.2022.139675](https://doi.org/10.1016/j.cplett.2022.139675).
- 67 V. Sivakumar and B. Rajamouli, Molecular Designing of Luminescent Europium-Metal Complexes for OLEDs: An Overview, *Phosphors*, 2018, pp. 325–404.
- 68 F. Weigend and R. Ahlrichs, Balanced basis sets of split valence, triple zeta valence and quadruple zeta valence quality for H to Rn: Design and assessment of accuracy, *Phys. Chem. Chem. Phys.*, 2005, **7**, 3297–3305, DOI: [10.1039/B508541A](https://doi.org/10.1039/B508541A).
- 69 F. Neese, The ORCA program system, *Wiley Interdiscip. Rev.: Comput. Mol. Sci.*, 2012, **2**, 73, DOI: [10.1002/wcms.81](https://doi.org/10.1002/wcms.81).
- 70 M. D. Hanwell, D. E. Curtis, D. C. Lonie, T. Vandermeersch, E. Zurek and G. R. Hutchison, Avogadro: An advanced semantic chemical editor, visualization, and analysis platform, *J. Cheminf.*, 2012, **4**, 1, DOI: [10.1186/1758-2946-4-17](https://doi.org/10.1186/1758-2946-4-17).
- 71 T. Koopmans, Über die Zuordnung von Wellenfunktionen und Eigenwertenzu den EinzelnenElektronenEines Atoms, *Physica*, 1934, **1**, 104–113, DOI: [10.1016/S0031-8914\(34\)90011-2](https://doi.org/10.1016/S0031-8914(34)90011-2).
- 72 R. Vijayaraj, V. Subramanian and P. K. Chattaraj, Comparison of global reactivity descriptors calculated using various density functionals: a QSAR perspective, *J. Chem. Theory Comput.*, 2009, **5**, 2744, DOI: [10.1021/ct900347f](https://doi.org/10.1021/ct900347f).

